Scientific Insights

Article

Acid-Activated Biochar From *Pinus elliottii* Pine Cone: Production, Characterization and High-Efficiency Adsorption of Methylene Blue

Matheus Antônio da Silva[1,2,*] **Iêda Aparecida Pastre Fertonani**[3] **and Clóvis Augusto Ribeiro**[2]

[1] EMBRAPA Environmnent, Jaguariúna CEP 13918-110, SP, Brazil
[2] Department of Analytical Chemistry, Physical Chemistry and Inorganic Chemistry, São Paulo State University (UNESP), Araraquara 14800-900, SP, Brazil
[3] Department of Chemistry and Environmental Science, São Paulo State University (UNESP), São José do Rio Preto 15054-000, SP, Brazil
* Correspondence: matheus.antonio-silva@unesp.br

Received: 4 November 2025; Accepted: 18 December 2025; Published: 29 December 2025

Abstract: The growing occurrence of emerging pollutants in wastewater demands sustainable and low-cost adsorbents. This study examines forest-residue strobili of *Pinus elliottii* as a biochar precursor for the removal of methylene blue from aqueous media. Unmodified biochars (P260, P300) were produced by torrefaction at 260 °C and 300 °C, respectively, while chemically activated samples (M260, M300) were obtained by H_3PO_4 impregnation (1:1, w/w) followed by identical torrefaction. Scanning electron microscopy coupled with EDS revealed pore-like surface features and minimal residual phosphorus after washing. FTIR spectra indicated a decrease in oxygen-containing groups and the development of more aromatic structures in the activated biochars. Batch adsorption experiments (25 °C, 0.2 g L^{-1}) showed that the Langmuir maximum capacity increased from 296.7 mg g^{-1} (P260) to 692.5 mg g^{-1} (M300). Kinetic profiles for M300 displayed a biphasic pattern: a rapid uptake within 6 h followed by a slower approach to equilibrium at 36 h, best fitted by a pseudo-second order model ($R^2 > 0.99$). Mixture design modelling (CCD) of P260/M300 blends identified an optimal formulation of 27–34 % M300 and 1770 min, achieving an adsorption capacity of 359.85 mg g^{-1}. The results demonstrate that moderate-temperature (300 °C) H_3PO_4 activation yields high-performance biochars that outperform anthracite coal and many reported biochars. Combining activated and non-activated fractions offers a viable strategy to maximise efficiency while mitigating potential phosphorus-related impacts. Biochar derived from *P. elliottii* strobili therefore emerges as a promising and sustainable option for treating cationic effluents.

Keywords: lignocellulosic residues, torrefaction, response surface methodology, low-cost adsorbent, environmental remediation, porous materials, carbon-based adsorbent

1. Introduction

Water pollution is one of the major environmental problems faced by modern society. Compounds originating from various anthropogenic activities are discharged into aquatic bodies, contaminating the environment and the organisms inhabiting these ecosystems [1]. The issue of water contamination, combined with the increasing water demand from human activities, contributes to the rising cost and complexity of treating water for human consumption, exacerbating the scarcity of potable water [2]. Among the most widely used methods for water and wastewater treatment is adsorption. Adsorption is one of the best-known separation and equilibrium processes and is also considered an effective approach for water decontamination and purification [3]. This process stands out due to its low initial cost, operational flexibility, ease of installation, sensitivity to toxic pollutants, and lack of harmful byproducts [4].

Methylene blue (MB) is not only a contaminant of environmental relevance but also a widely recognized spectrophotometric probe [5]. MB removal is widely adopted as a benchmark for evaluating the efficiency of carbon-based adsorbents and is recognized as a model cationic contaminant due to its defined charge, aromaticity, and well-characterized interaction mechanisms with carbonaceous surfaces, allowing adsorption trends to be extrapolated to a wide range of positively charged organic pollutants [6,7]. Anthracite coal (C_{ant}) is a traditional adsorbent for MB due to its high fixed carbon content, rigidity, and porosity, but its use is increasingly questioned because of its environmental impacts. Open-pit mining generates severe ecological degradation, including acid mine drainage and elevated metal concentrations in surrounding waters. After use, coal residues and combustion ashes pose long-term contamination risks through the leaching of toxic elements such as As, Hg, and Cd [8-10]. These limitations underscore the need for more sustainable alternatives.

Biochar emerges as a promising substitute due to its greater technical, economic, and environmental feasibility [11,12]. It is a carbonaceous solid obtained through thermal decomposition of biomass under oxygen-limited conditions, generating a low-density material rich in carbon and characterized by a stable porous structure [13]. The biomass used for biochar production is highly diverse and includes agro-industrial residues such as husks, leaves, straw, and bagasse, as well as organic and lignocellulosic wastes from the food industry and other sectors [14]. A scientometric review of 2,673 articles shows exponential growth in biochar applications for wastewater treatment, particularly in target-specific adsorption systems [15]. Biochar and other adsorbents have achieved high removal efficiencies for emerging pollutants, including pharmaceuticals, hormones, and microplastics, often exceeding 90% [16]. While bio-based adsorbents are low-cost and environmentally compatible, challenges such as regeneration and stability remain [17]; polymeric and magnetic composites offer higher performance but may involve higher costs or risks of metal leaching [17,18]. Functionalized carbons and activated biochars combine high surface area and selectivity, though some chemical activators raise environmental concerns [19-22].

The strobili of *Pinus elliottii* are an example of biomass suitable for biochar production. These reproductive structures of pine trees, once dried at the end of their life cycle, are often discarded in large quantities due to the lack of appropriate end-use applications, thereby becoming a residue. Composed predominantly of cellulose, hemicellulose, and lignin, strobili biomass is well suited for the production of biochar and its use as an adsorbent for dyes, exhibiting physicochemical properties favorable to environmental applications, including high porosity, surface area, and carbon content [23-25]. These characteristics make it a promising material not only for pollutant removal from wastewater but also for energy recovery and soil amendment [26].

Biochars can undergo pre-, during-, or post-thermal decomposition treatments that promote structural, surface, and/or physicochemical modifications. These treatments are referred to as activation processes, and they aim to enhance the adsorptive capacity of the material and to functionalize its pores, increasing its selectivity toward specific target compounds [27]. Activation can be physical, such as drying, grinding, and sieving, or involve the introduction of activating gases post-thermal decomposition to clear blocked pores. In chemical activation, chemical agents are impregnated into the biomass or biochar [28,29].

Chemical activation with acids, bases or oxidizing agents are commonly applied before pyrolysis, allowing controlled surface corrosion that enhances porosity and reactivity [30-32]. Among these agents, phosphoric acid (H_3PO_4) is one of the most widely used due to its effectiveness and comparatively lower environmental impact than $ZnCl_2$ or KOH [6,28,29,33]. H_3PO_4 promotes pore development and introduces oxygenated functional groups, substantially increasing adsorption capacity [34,35]. Variants such as $H_3PO_4 + H_2O_2$ activation or combinations with physical/steam activation further improve pore structure while reducing post-activation residues [36,37]. Studies consistently show strong gains after phosphoric acid modification; for example, increases of 1.4- to 5-fold in Pb^{2+} and Cd^{2+} adsorption [12], up to eight-fold increases in surface area in agro-industrial residues [38], and enhanced metal uptake through electrostatic attraction, π-interactions, and complexation with P=O groups [39-41]. The present study also evaluates mixtures of phosphoric-acid–activated and unmodified biochars as a strategy to enhance adsorption capacity while reducing chemical usage and minimizing the environmental risks associated with excess acid activation.

In light of these considerations, the present work investigates the adsorption performance of strobilus-derived biochars produced at two torrefaction temperatures (260 and 300 °C), both with and without phosphoric acid activation, as well as mixtures of these materials. Using MB as a model cationic pollutant under controlled batch conditions, the study evaluates equilibrium isotherms, adsorption kinetics, and mechanistic behavior while comparing the materials to previously reported activated biochars. To the best of our knowledge, no previous work has simultaneously assessed low-temperature biochars, their phosphoric-acid-activated derivatives, and mixed formulations for dye adsorption. This approach allows the identification of environmentally safer and potentially scalable biochar systems for contaminant removal.

2. Materials and Methods

2.1. Materials

2.1.1. Collection and Preparation of Pine cone Biomass Samples

Pinecone samples were collected from the Botanical Garden Forest (21°45'12.4"S, 48°10'58.4"W), located in the city of Araraquara, São Paulo, Brazil. The samples were washed with deionized water, cleaned, and air-dried. After drying, the material was ground using a rural knife mill (JF® 5D), sieved, and stored for biochar production; the pinecone biomass was denominated P0.

2.1.2. Preparation and Modification of Pine cone Biochars

The biochars were produced by torrefaction of pinecone biomass. The biomass was placed in an oxygen-restricted container and torrefied in a muffle furnace (EDG—EDGCON® FV-2-EDG), with a heating rate of 10 °C min^{-1} up to 260 °C and a residence time of 60 minutes. After torrefaction, the resulting biochar was washed with deionized water until the biochar reached stability in water. The biochar was dried in an oven at 105 °C, and sieved through a 60-mesh sieve.

To produce the H_3PO_4–modified pine cone biochar, the biomass was first chemically activated with the acid and then torrefied, following the procedure described by Yangmur (2008) with modifications [29]. Twenty grams of pine cone biomass were mixed with an 85% phosphoric acid (Synth®) solution in a 1:1 mass ratio and stirred in an orbital shaker (Marconi® MA830/SR) for 72 hours at 25 ^{0}C and the acrylic lid of the orbital shaker was covered with adhesive paper to create a dark environment. After the contact period, the biomass was washed with deionized water, dried in an oven at 105 °C, and sieved through a 60-mesh screen.

The torrefaction procedure was the same as for unmodified pine cone biomass, with a heating rate of 10 °C min^{-1} up to 260 °C and a residence time of 60 minutes, repeated washing with deionized water until the biochar reached stability, dried in an oven at 105 °C, and sieved through a 60-mesh screen. The acid-modified biomass was divided into two portions and torrefied at 260 °C and 300 °C, respectively. The resulting biochars were labeled M260 and M300.

2.1.3. Methylene blue solution

A 1000 mg L^{-1} (≈3.126×10^{-3} mol L^{-1}) stock solution of MB (Sigma-Aldrich®, 97%) was prepared by dissolving 1.000 g of MB (equivalent to 100% purity) in 1.00 L of deionized water. This solution was used for subsequent isotherm and kinetic analyses. Calibration curves for determining the molar extinction coefficient (ε) were obtained from spectrophotometric measurements of MB solutions (from 1.00 to 30.00 mg L^{-1}). Samples were prepared by adding 3.0 mL of solvent to a cuvette and spiking microliter volumes of the stock solution. After vortex homogenization, the absorbance was recorded in a UV-Vis single-wavelength spectrometer (Micronal® B582), and the calibration curve was constructed using the maximum absorbance wavelength of the monomeric species (665 nm in aqueous solution) [11], where the ε was applied to convert absorbance values into MB concentration using the Beer-Lambert Law [22].

A representative calibration curve obtained is shown in Figure 1a. The curve showed excellent linearity ($R^2 = 0.9989$) and was therefore chosen as the representative calibration. The corresponding residual plot (Figure 1b) confirms that residuals are randomly distributed around zero with no systematic deviations, demonstrating the adequacy of the Beer–Lambert linear model across the full concentration range.

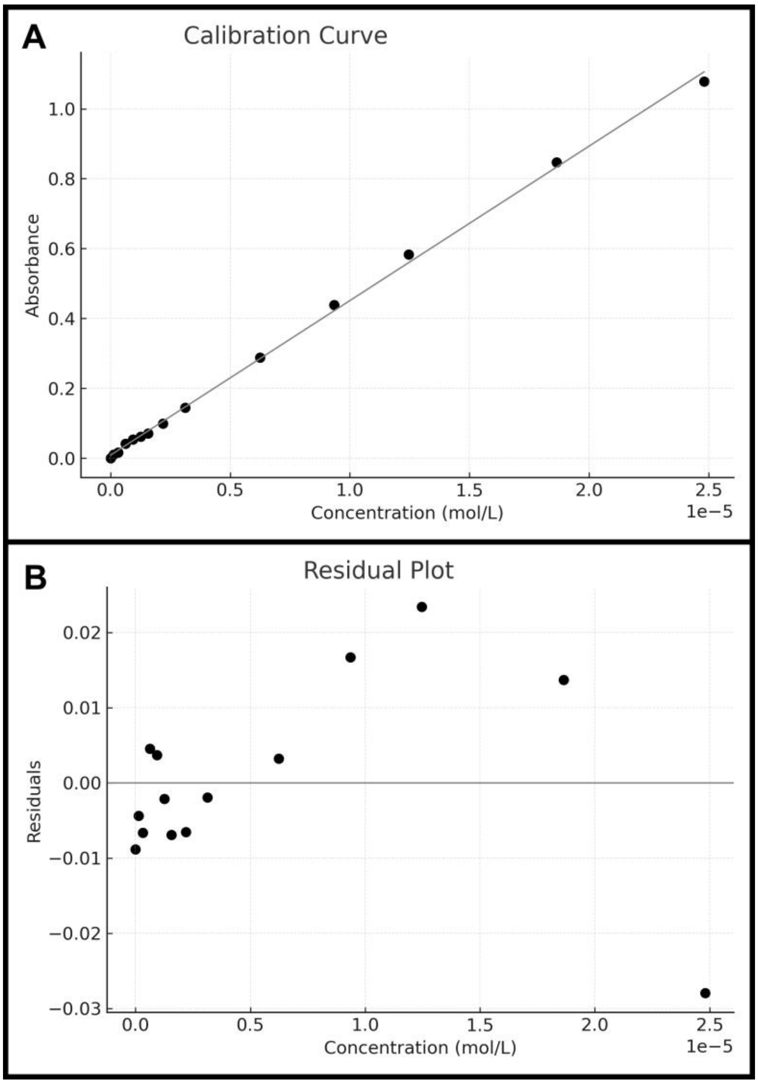

Figure 1. Calibration curve for methylene blue (MB) at 665 nm and (b) Residuals of the linear regression for the calibration curve.

2.2. Characterization of Materials

Infrared absorption spectroscopy was conducted in the mid-infrared region for samples P260, P300, M260, and M300. The spectra were recorded from 4000 cm^{-1} to 400 cm^{-1}, with a spectral resolution of 1.0 cm^{-1}, with each result being the average of two spectra, each acquired with 16 scans. The analysis was performed using a BRUKER Hyperion 2000 instrument equipped with an ATR (Attenuated Total Reflectance) accessory, without the use of potassium bromide (KBr) pellets.

Field Emission Scanning Electron Microscopy (FEG-SEM) analysis was carried out for samples P0, P260, P300, M260, and M300 to observe the surface morphology of the materials. Energy-dispersive X-ray spectroscopy (EDS) was used to estimate the atomic composition of the material surfaces. SEM imaging was performed using a JEOL® JSM-7500F microscope, equipped with a Thermo Scientific® UltraDry EDS detector with an accelerating voltage of 10.00 keV, working distance of 5.0 mm without coating and magnification rate from 1000x to 20000x. The point of zero charge (pHPZC) of the biochars was determined using the pH-drift method, following procedures described in the literature for phosphoric acid–activated carbons [34].

2.3. Methylene Blue (MB) Adsorption on Biochar

In order to observe the asorption behavior of MB in the biochars, adsorption isotherms were determined through batch equilibrium experiments using P260, P300, M260, M300, and C_{ant} as adsorbents and methylene blue as the spectrophotometric probe. The tests were conducted with a fixed adsorbent concentration of 0.2 g L^{-1} in a fixed volume of deionized water, while varying the MB concentration from 1.56×10^{-6} to 1.25×10^{-5} mol L^{-1} for P260 and P300, and from 1.56×10^{-6} to 3.10×10^{-5} mol L^{-1} for M260 and M300. Volumes ranging from 25 to 200 µL for P260 and P300, and up to 500 µL for M260 and M300 were added to 50 mL of deionized water, with an adsorbent-only blank containing only the biochar and water. The systems were shaken at 200 rpm and 25 °C under dark conditions to minimize photolysis of MB.

The systems were centrifuged at 2500 rpm for 20 min to separate the solid and liquid phases. Subsequently, spectrophotometric measurements of the liquid phase were performed using a UV-Vis spectrophotometer at 665 nm. All experiments were performed in quadruplicate, and the adsorbent-only blank was used as the baseline.

Adsorption kinetics were evaluated using P260 and M300 as adsorbents and MB as the probe molecule. Batch kinetic experiments were conducted with fixed concentrations of each adsorbent (0.2 g L^{-1}) and MB (1.55×10^{-5} mol L^{-1} for P260 and 2.55×10^{-5} mol L^{-1} for M300) in a constant volume of deionized water, with varying contact times. The systems were placed on a shaker at 200 rpm and 25 °C also under dark environment, with equilibrium times ranging from 5 minutes to 24 hours for P260 and up to 36 hours for M300. After the contact time, the phases were separated, and absorbance readings were performed as in the isotherm tests. Each experiment was conducted in triplicate for both P260 and M300.

2.4. Adsorption Isotherm Models and Isotherm Classification

To better elucidate the MB adsorption process on the materials, the experimental adsorption isotherms were fitted to adsorption models to obtain data on capacity and adsorption thermodynamics. In this study, four adsorption isotherm models were used: the Langmuir, Freundlich, Dubinin–Radushkevich (DRK) and Temkin models.

The Langmuir adsorption model describes a process in which each adsorbed molecule interacts with only one adsorption site and does not interact with other adsorbed molecules. The adsorbent surface is assumed to have a fixed number of identical energy sites. This model allows for the quantification of monolayer adsorption capacity and provides a qualitative assessment of the favorability of the adsorption process [20,42].

The Freundlich adsorption model is a more general model that assumes a heterogeneous adsorption process, which may occur in multiple layers. It is an empirical model that considers potential cooperative interactions among adsorbed molecules or with heterogeneous surfaces with adsorption sites of varying energies. This model provides only qualitative parameters, unlike the Langmuir model, which provides quantitative values [7,20].

The DRK model is a semi-empirical model, adapted from the Polanyi adsorption theory, which considers van der Waals forces as predominant in the adsorption process. The DRK model provides quantitative estimates of adsorption capacity and adsorption free energy, allowing one to assess whether the process is exothermic and spontaneous [43].

The Temkin adsorption model assumes that the heat of adsorption of all molecules in the layer decreases linearly with surface coverage, due to adsorbate–adsorbate interactions. This model considers a uniform distribution of binding energies up to a maximum value and is therefore suitable for systems in which adsorbent–adsorbate and adsorbate–adsorbate interactions play a significant role. The model provides the Temkin constants related to the equilibrium binding strength and the variation in adsorption energy, allowing a semi-quantitative assessment of the interaction intensity between MB molecules and the adsorbent surface [4,20,43].

Giles′ classification system was also used to characterize the isotherm shapes. For this, the adsorption isotherms were plotted with the amount of MB adsorbed per unit mass of adsorbent on the y-axis and the equilibrium concentration on the x-axis [44]. Based on the comparison with the Giles classification system, isotherms can be grouped into four types: Langmuir type (L), S-type (sigmoidal), high-affinity type (H), and partition coefficient type (C).

2.5. Adsorption Kinetic Models

Similar to the equilibrium isotherms, adsorption kinetic models were used to gain further insight into the adsorption process. The following models were employed: Lagergren or pseudo-first-order, pseudo-second-order, intraparticle diffusion (Fick′s law), and the Elovich model.

The Lagergren model is widely used in solid-liquid systems and is based on the derivative of adsorption capacity over time [7,20]. The pseudo-second-order kinetic model also considers adsorption capacity over time but incorporates a quadratic relationship [45].

The intraparticle diffusion model assumes diffusion as the primary transport mechanism, with the adsorption rate varying with the square root of time [7]. The Elovich model was originally developed for gas adsorption on solids and is based on the balance between the initial adsorption rate and the desorption rate [20,43,44].

2.6. Statistical Planning of Experiments with Modified and Unmodified Biochar Mixtures

To optimize the removal efficiency of MB using mixtures of unmodified biochar (P260) and modified biochar (M300), multivariate analyses were performed to identify the optimal parameters for modified biochar percentage and equilibrium time. A Central Composite Rotational Design (CCD), a factorial design model commonly used for process optimization [46], was applied to determine the best MB removal conditions.

The software Statistica 12.0 (TIBCO Software Inc.) was used both for the experimental design and for the statistical analysis of the resulting data. The CCD data for the responses were fitted to a second-order polynomial response-surface model by multiple linear regression using the ordinary least-squares method, and model significance, individual coefficients, and lack-of-fit were evaluated by analysis of variance (ANOVA) and Student′s t-test at a 95% confidence level.

The factors evaluated in the design were the percentage of M300 in the total adsorbent mass (%M300) and the equilibrium time (t) between the adsorbents and the MB solution. Equilibrium times were selected based on prior kinetic experiments. However, since M300 displayed biphasic adsorption phases, two separate multivariate analyses were performed: one focusing on shorter equilibrium times (with 360 minutes as the central point) and another focusing on longer times (with 1380 minutes as the central point). The factors tested are presented in Table 1, and each experiment was conducted in triplicate.

Table 1. Factors tested in CCD experiments

	CCD 360 minutes		CCD 1380 minutes	
Normalized values	Contact time (min)	% M300	Contact time (min)	% M300
-1,41 ; 0	127	20	600	20
+1 ; -1	525	10	1896	10
0 ; 0	330	20	1380	20
-1 ; +1	195	30	864	30
0 ; 0	330	20	1380	20
-1 ; -1	195	10	864	10
0 ; 0	330	20	1380	20
+1 ; +1	525	30	1896	30
0 ; +1,41	330	34,14	1380	34,14
+1,41 ; 0	583	20	2160	20
0 ; -1,41	330	5,86	1380	5,86

The evaluated responses were the experimental adsorption capacity (Qe) and the difference between the experimental and theoretical adsorption capacities (Qe − Qt), the latter being derived from P260's kinetic adsorption data.

The adsorption experiments were carried out similarly to the kinetic tests with P260. The adsorbent and dye concentrations were fixed at 0.2 g L^{-1} and 1.55×10^{-5} mol L^{-1}, respectively, with %M300 and equilibrium time as the variable factors. The experimental adsorption capacity at equilibrium (Qe) was calculated according to Equation (1), one of the responses in the multivariate analysis:

$$Qe = (C_o\text{-}C_e)\ V / m \qquad (1)$$

where C_0 = initial MB concentration in solution (mg L^{-1}); C_e = MB concentration in solution after equilibrium time (mg L^{-1}); m = mass of adsorbent (g); V = volume of the solution (L). The second evaluated response (Qe − Qt) compares the experimental capacity with the theoretical capacity obtained from the kinetic model of unmodified biochar (P260). If the difference (Qe − Qt) is greater than zero, it indicates that the addition of modified biochar (M300) had a positive influence on the overall adsorption performance.

3. Results and Discussion

3.1. Scanning Electron Microscopy (SEM)

The SEM images of pinecone biomass, P260, P300, M260, and M300 are shown in Figure 2. These images reveal that the torrefaction process induces significant changes in the surface morphology of the materials. Torrefaction at 260 °C results in a smoother and more uniform surface compared to the raw biomass, while torrefaction at 300 °C leads to the formation of a rougher and more irregular surface texture.

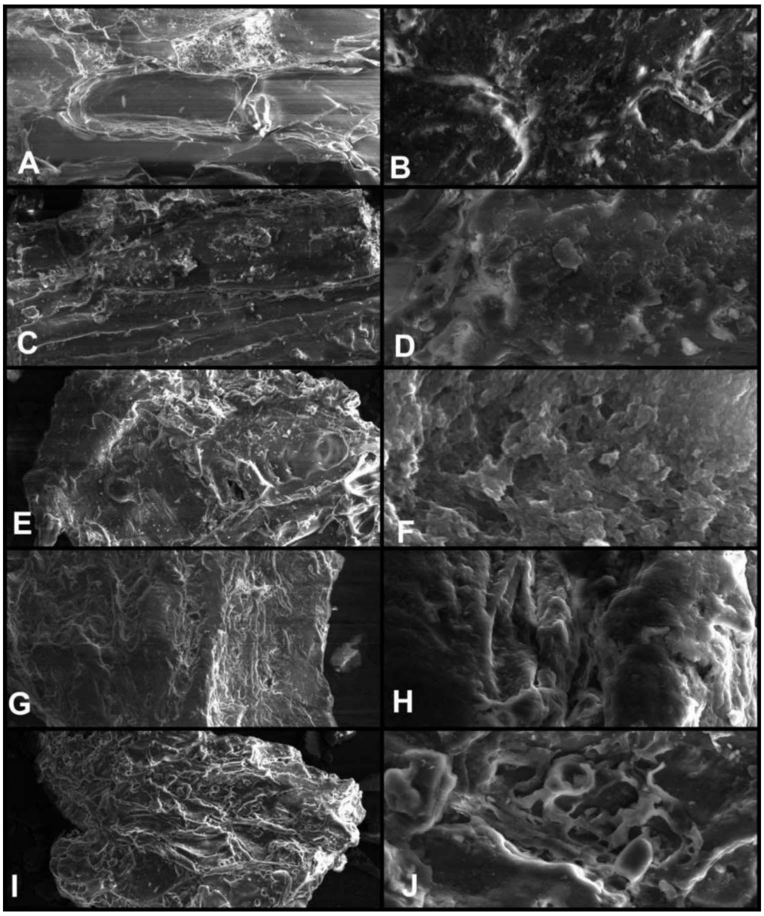

Figure 2. Scanning electron microscopy images of pinecone biomass (a, b), P260 (c, d), P300 (e, f), M260 (g, h), and M300 (i, j), with magnifications of 1000x (a, c, e, g, I) and 10000x (b, d, f, h, j).

The acid pretreatment of the biomass promotes surface leaching, as phosphoric acid oxidizes part of the surface carbon in the biochar, partially degrading it. The combination of acid pretreatment and torrefaction leads to a rougher and more heterogeneous surface with a greater number of surface irregularities when compared to biochars produced without pretreatment [7,24,34]. Biochars with less uniform and rougher surfaces are often associated in the literature with the development of pore-like structures and the potential for higher surface area and pore volume, which are key characteristics for achieving more efficient adsorbents in the removal of aqueous contaminants [18,37]. In the present study, these inferences are based solely on morphological observations (SEM), and no direct BET surface area or pore size distribution measurements were performed, which is acknowledged as a limitation [1,32].

According to the EDS spectra (Figure 3), the atomic composition of the modified biochars is primarily composed of carbon and oxygen, with smaller amounts of inorganic elements such as calcium, magnesium, silicon, and potassium. Phosphorus was detected only in M300, with approximately 0.1% content, indicating that the washing steps effectively removed nearly all of the phosphorus used during the pretreatment process.

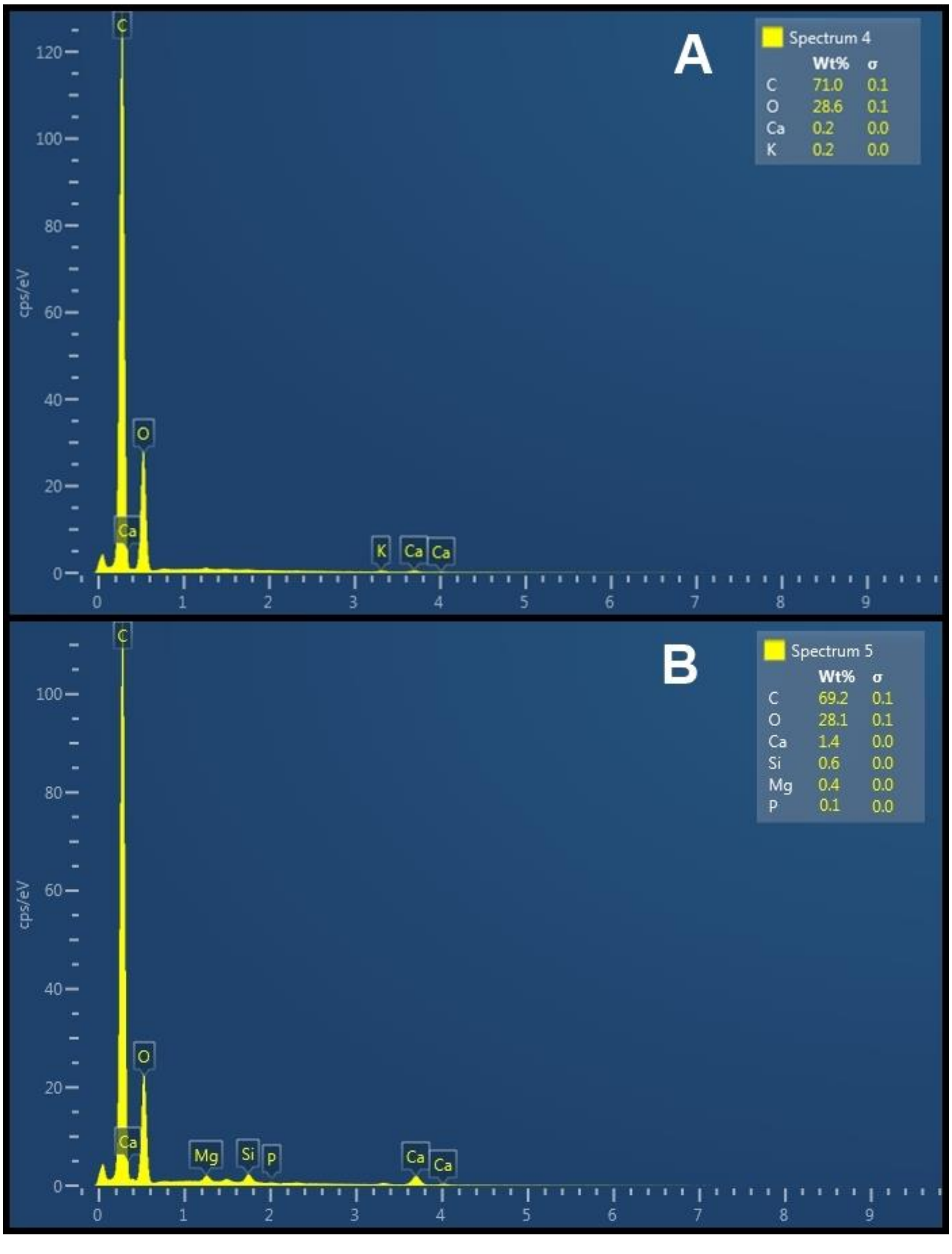

Figure 3. EDS spectra of M260 and M300

3.2. Fourier Transform Infrared Spectroscopy (FTIR)

The infrared spectra of P260, P300, M260, and M300 are shown in Figure 4. The unmodified biochars exhibited several characteristic bands of biochars derived from pinecone biomass, including: broad bands with maxima at 3300 cm⁻¹ and 2926 cm⁻¹, attributed to hydrogen bonds and CH_2 groups present in the organic matter of the biomass [47,48]; three sharp bands at 1704, 1591, and 1512 cm⁻¹, attributed to the overlapping stretches of C=O and C=C in carboxylic groups [49]; and several small bands between 1434 and 1155 cm⁻¹, characteristic of aromatic ring bonds in lignocellulosic materials, culminating in a broad band at 1023 cm⁻¹, attributed to C–O bonds, mainly found in glucose monomer linkages of cellulose and hemicellulose [47,48]. In P260, bands related to hydrogen bonding at 3300 cm⁻¹ and C–O bonds from lignocellulosic material at 1023 cm⁻¹ are more prominent, while P300 shows higher transmittance in bands attributed to C=O and C=C of carboxylic acids and aromatic rings from lignocellulosic materials.

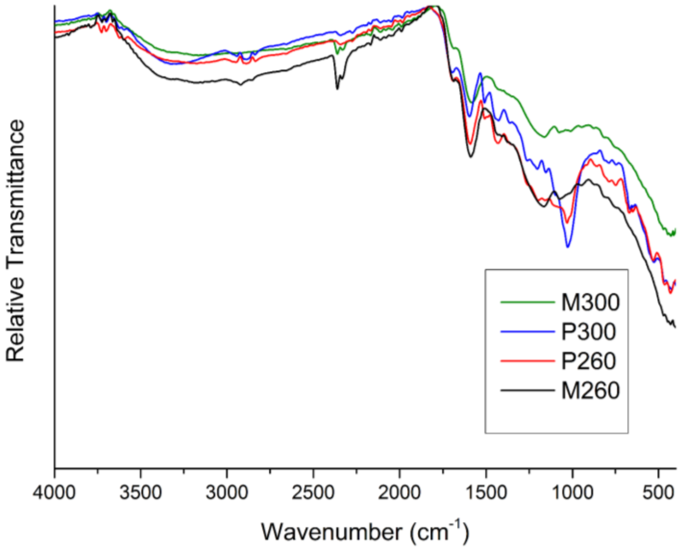

Figure 4. Infrared spectra of modified and unmodified biochars

In the modified biochars, spectral changes indicative of chemical activation were observed, such as a slight intensity reduction after activation, which may indicate partial matrix dehydration or hydroxyl group consumption during the modification process [34,37,50]. The hydrogen bonding bands broadened, and a new band appeared at 2340 cm⁻¹, attributed to CO_2 adsorbed from the air [48]. The bands between 1450 and 1000 cm⁻¹ were broader and less intense, with poorly defined peaks, culminating in a broader band at 1159 cm⁻¹, related to C–O bond vibrations in the internal structure of cellulose and hemicellulose, which appeared only as a shoulder in the unmodified biochar spectra.

FTIR analysis also revealed the absence of an intense band in the 1230–1260 cm⁻¹ range, typically attributed to P=O or P–O–C bonds. This absence indicates negligible retention of phosphorus in the carbonaceous surface, in agreement with EDS results [7,50]. Comparison between the spectra of P260 and P300 (unmodified biochars) shows similar profiles, with well-defined bands associated with oxygenated groups such as –OH (~3430 cm⁻¹), C–H (~2920 cm⁻¹), and C–O (~1030 cm⁻¹) [48,49]. However, after activation with H_3PO_4, these bands were substantially attenuated in M300, with reduced peak intensities and broader bands [37,50]. This pattern suggests that the activation process in the biochar produced at 300 °C promoted more extensive removal of surface functional groups, possibly due to lower thermal stability and higher residual reactivity compared to the 260 °C biochar [37,45-51].

Therefore, the modification of the 300 °C biochar appears to have resulted in a more degraded surface with fewer functional groups detectable by FTIR. In contrast, M260, although also subjected to the same activation process, retained more evident signals of surface functionalities, indicating a less aggressive modification. These results support the hypothesis that modification efficiency depends not only on the chemical agent but also on the biochar's pre-existing structure, which is directly influenced by torrefaction temperature [37,50].

Additionally, the surface charge was evaluated by the pHPZC method. The biochars modified and without modification exhibited pHPZC values close to neutrality (between 5.4 and 6.5), indicating predominantly neutral to slightly negative surfaces under the experimental conditions. This behavior supports the occurrence of electrostatic attraction with the cationic MB molecules [34,43].

3.3. Methylene Blue Adsorption Isotherms

The adsorption isotherms of MB onto P260, P300, M260, M300, and C_{ant} are shown in Figure 5. It was observed that the phosphoric acid pretreatment increased the adsorption capacity of the biochars. The highest total adsorption in the monolayer across all MB concentrations tested was M300, reaching approximately 652.6 mg g^{-1}. M260 ranked second, with an adsorption in the monolayer close to 501.1 mg g^{-1}. The increase in MB adsorption in the monolayer of M260 compared to P260 was 370%, while for M300, it was 1200% compared to P300. Regarding adsorption performance, P260 showed higher adsorption in the monolayer than C_{ant} at higher MB concentrations, whereas P300 presented the lowest adsorption in the monolayer across all concentrations tested. The adsorbent-only blank did not show significant absorbance (>0.007 Uabs) in all adsorbents used in the isotherms.

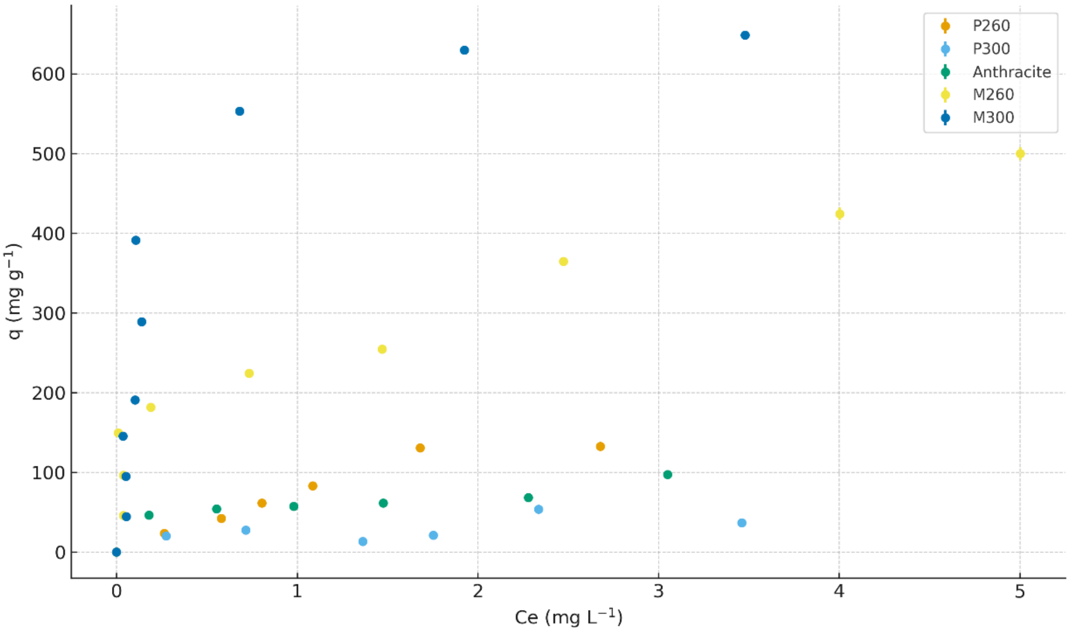

Figure 5. Adsorption isotherms of MB onto C_{ant}, P260, P300, M260, and M300.

According to the Giles classification system, the isotherms of P260 and P300 were identified as type L (Langmuir type), indicating favorable dye–adsorbent interaction. However, P300 exhibited a lower affinity for MB than P260, as evidenced by its smaller initial adsorption increase and lower plateau value. The MB adsorption isotherms for M260 and M300 were classified as type H (high-affinity), indicating that the adsorption of MB onto these adsorbents was highly favorable, resulting in high adsorption capacities.

The application of adsorption isotherm data to adsorptive models is presented in Tables 2 and 3. The isotherm data for P260 showed a stronger correlation with the Langmuir, Freundlich and Temkin models, while the data for C_{ant} and the modified biochars correlated better with the DRK model. P300, however, did not correlate significantly with any of the applied models.

Table 2. Adsorption parameters of Langmuir and Freundlich.

	Langmuir			Freundlich		
	R2	Qmax (mg g-1)	KL (L mg-1)	R2	Kf (mg L-1/n g-1/n)	n
P260	0.9356	274.68	0.4005	0.9146	3.7913	1.516
P300	0.6161	229,029	$4.0056\ 10^{-6}$	0.6272	0.7545	0.826
C Ant	0.4692	86.18	3.7363	0.6861	3.1559	3.401
M260	0.7654	508.02	1.2698	0.9158	13.5189	3.001
M300	0.9074	685.72	5.8996	0.8411	24.7619	3.341

Table 3. Adsorption parameters of DRK and Temkin isotherms.

	DRK			Temkin		
	R2	Q0 (mg g-1)	β	R2	B	KT
P260	0.6113	2.9365	-0.1254	0.9304	5.1114	1.1418
P300	0.6078	0.9166	-0.115	0.6161	8011.5846	0.000114
C_ant	0.9351	2.4821	-0.0855	0.6163	0.8266	50.7785
M260	0.7181	9.1461	-0.0433	0.8387	4.1897	33.9525
M300	0.3892	13.8946	-0.0757	0.8828	6.5609	58.7376

The strong fit of P260 across multiple models indicates that P260 possesses a surface with relatively well-distributed adsorption sites, yet still exhibits enough energetic heterogeneity for models such as Freundlich and Temkin to accurately describe its behavior [4,20,43]. The Langmuir Qmax indicates a relatively high monolayer adsorption capacity for a low-temperature biochar, while the moderate KL value suggests a balanced adsorption affinity without strongly irreversible binding [14,24,36]. The Freundlich exponent $n \approx 1.52$ confirms a heterogeneous surface with favorable adsorption ($n > 1$), consistent with the presence of varied oxygenated functional groups [27,32,37,43]. The Temkin parameters (B = 5.11; KT = 1.14) indicate that the adsorption energy decreases gradually with increasing surface coverage rather than abruptly, reflecting a material in which interactions between the adsorbate and the surface remain moderate and energetically consistent [20]. Such a combination suggests a mixed adsorption mechanism, involving both regions that behave similarly to monolayer adsorption and others with varying affinity, which is typical of low-temperature biochars enriched in oxygenated functional groups and characterized by partially disordered microstructures. In contrast, the Dubinin–Radushkevich (DRK) model provided a significantly weaker fit for P260 ($R^2 = 0.611$), indicating that adsorption in this material does not follow the assumptions of uniform physical adsorption with a Gaussian distribution of adsorption energies, suggesting the adsorption mechanism in P260 is not dominated by classical physisorption but instead reflects a more complex energetic landscape [5,43].

The C-ant biochar showed its strongest fit with the DRK isotherm, indicating that its adsorption behavior closely follows a physisorption-dominated mechanism with a relatively uniform energetic distribution of micropores and implies that C-ant possesses a more homogeneous pore network and less surface heterogeneity compared to the other biochars, likely reflecting a smoother carbon matrix and a lower density of oxygenated functional groups. The DRK parameters support this interpretation: the q_0 value of 2.48 mg g^{-1} reflects a moderate theoretical adsorption capacity associated with microporous filling, while the negative β coefficient (–0.0855) suggests a low mean adsorption energy, consistent with weak physical interactions rather than chemisorption [4,20,43].

In contrast, the P300 biochar did not correlate well with any of the four isotherm models applied. All coefficients of determination were low ($R^2 < 0.63$ for Langmuir, Freundlich, Temkin, and DRK), and several fitted parameters were physically unrealistic—such as extremely high Qmax estimates or unstable Temkin constants. This poor model performance suggests that the adsorption behavior of P300 does not follow any classical equilibrium pattern. Overall, the inability of P300 to fit established isotherm models reinforces that its interaction with the adsorbate is weak, inconsistent, and not governed by well-defined adsorption mechanisms [6].

The phosphoric acid treatment modified the surface of the biochar, making it more homogeneous. As a result, the adsorption process aligns more closely with the Langmuir model, more similar to that of C_{ant}, which assumes a uniform surface with sites of equal energy and monolayer adsorption [27,36]. The M260 biochar exhibited adsorption behavior that parallels several of the trends observed for P260, where both materials showed their best performance in models that incorporate surface heterogeneity, such as the Freundlich ($R^2 = 0.718$ for M260; 0.915 for P260) and Temkin isotherms ($R^2 = 0.839$ for M260; 0.930 for P260), indicating that 260 °C chars generally possess diverse adsorption sites shaped by abundant oxygenated functional groups and partially developed microstructure [8]. However, M260 displayed higher adsorption capacity (Langmuir Qmax ≈ 492 mg g^{-1}) compared to P260 (Qmax ≈ 274.68 mg g^{-1}), suggesting that the modified material has a more accessible pore network or greater availability of active sites despite both being low-temperature chars [24,27,50]. Overall, the comparative analysis indicates that although P260 has more balanced and consistent model fitting, M260 provides higher capacity, reflecting structural differences between the two biochar precursors despite identical torrefaction conditions.

In contrast, M300 biochar showed strong adsorption model performance that differs sharply with its pair P300, despite both being produced at the same torrefaction temperature. While P300 exhibited poor correlation with all four isotherms and generated several physically unrealistic parameters, M300 achieved excellent fits, including Langmuir ($R^2 = 0.987$) and Temkin ($R^2 = 0.883$). This divergence indicates that the structural and chemical characteristics of the two precursors respond very differently to thermal decomposition at 300 °C. For M300, the high Qmax (685 mg g^{-1}) and Temkin constants (B = 6.56; KT = 58.74) reflect a surface with increasing aromatic condensation and a more ordered pore architecture, enabling predictable and energetically stable adsorption [5,14,32]. Thus, although P260 and M260 shared similar qualitative patterns at 260°C, the jump to 300°C produced markedly different outcomes, where M300 becomes one of the best-performing materials while P300 becomes the least model-compliant biochar in the dataset. Wang et al. (2020), using sugarcane bagasse pyrolyzed at 500 °C, observed an increase in MB adsorption capacity from 158.7 to 588.2 mg g^{-1} with activation (approximately 270%) [1]. Peng et al. (2017), using pine sawdust activated at 450 °C, obtained Q_{max} values close to 500 mg g^{-1} for Cu^{2+} and Cd^{2+} [51]. Zhang et al. (2020), with rice straw activated at 600 °C, reported an increase from 128.1 to 416.7 mg g^{-1} (about 225%) in malachite green adsorption [52].

The higher activation efficiency observed in this study may be attributed to the lower temperature used in biochar production (300 °C), which favors the preservation of oxygenated functional groups in the biomass, such as –OH and –COOH, enhancing reactivity with phosphoric acid. This greater chemical interaction promotes more extensive pore opening and surface functionalization during activation. In comparison, Wang et al. (2020) used 500 °C and achieved a 270% increase in MB adsorption [1]; Zhang et al. (2020), with pyrolysis at 600 °C, reported a 225% increase for malachite green [52]. Although Peng et al. (2017) observed increases over 5000% for Cu^{2+} and Cd^{2+} adsorption, their pyrolysis temperature was 450 °C and the initial adsorption values were very low, amplifying the percentage gain [51]. These results suggest that higher pyrolysis temperatures, while still effective, may limit the efficacy of chemical treatment due to increased condensation of the carbon structure. Thus, moderate temperatures for biochar production, combined with acid activation, may be a more efficient strategy for producing high-performance adsorptive biochars.

Therefore, M300 stands out as the best modified adsorbent due to its higher adsorption capacity and more significant improvement compared to its torrefied but untreated counterpart. Among the untreated adsorbents, P260 demonstrated the best adsorption performance relative to P300.

3.4. Adsorption Kinetics

The results of MB adsorption kinetics for P260 and M300 are presented in Figures 6a and 6b, respectively. It is evident that the two adsorptive processes exhibit distinct behaviors. For P260, equilibrium in the adsorption process was achieved between 360 and 540 minutes, with the adsorption capacity at equilibrium being similar to that observed in the adsorption isotherm studies. This rapid approach to equilibrium is consistent with the Boyd plot (Figure 6c), in which the Bt versus t relationship is linear and passes close to the origin in the first 240–360 min, indicating that film diffusion is the main rate-controlling step for P260.

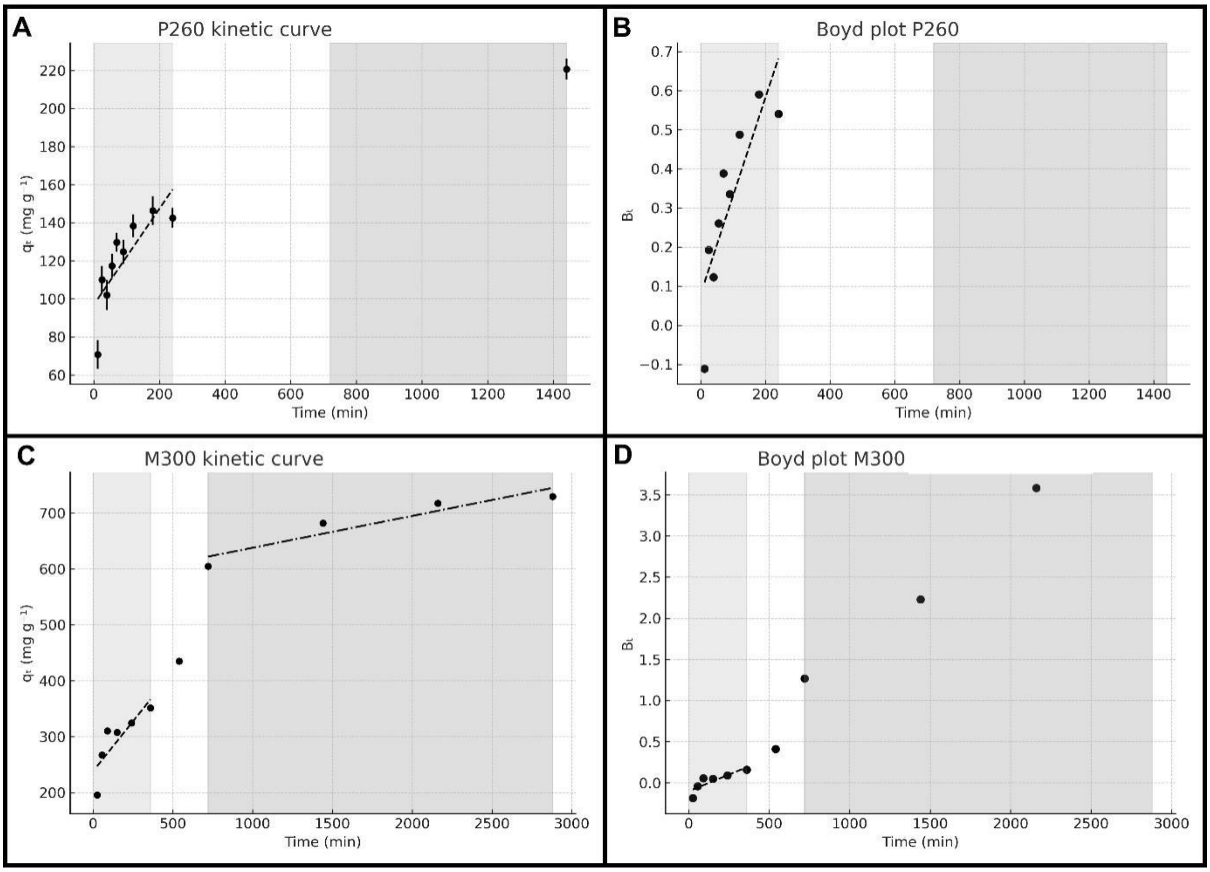

Figure 6. Adsorption kinetics of methylene blue (MB) in (a) P260 and (c) M300, with the Boyd plots (b) and (d), respectivelly.

In the case of M300, different adsorption plateaus were observed. An initial apparent plateau is reached within 360 minutes, after which the adsorbed concentration increases again. A second plateau occurs up to around 1500 minutes, with the adsorbed concentration continuing to rise slowly until stabilizing at 2160 minutes (36 h). This final adsorption plateau corresponds to an adsorbed concentration comparable to the maximum observed in the isotherm studies and is approximately five times higher than that of P260. The kinetic profile of M300 therefore shows a biphasic adsorption behavior: a first, faster stage up to about 6–12 h, followed by a slower uptake phase extending up to 24–36 h. This interpretation is supported by the Boyd plot for M300 (Figure 6d), where Bt is approximately linear only in the initial region (up to ≈360 min), while the subsequent deviation from linearity and the appearance of a non-zero intercept indicate a progressive transition from film-diffusion control to intraparticle diffusion in the slower second stage, which becomes evident after 12 h.

Importantly, this two-stage kinetic behavior is not inconsistent with the fact that the equilibrium data for M300 are better described by Langmuir and Temkin isotherms. Equilibrium isotherm models describe how adsorption sites are occupied at the final state, whereas kinetic models and Boyd analysis describe the sequence of rate-limiting steps along the pathway to equilibrium. Similar combinations of Langmuir-type equilibrium with diffusion-controlled or multi-stage kinetics have been reported for carbonaceous adsorbents and diffusion models applied to porous solids, where a fast film-diffusion step is followed by slower intraparticle diffusion or pore-filling processes [5,45].

Many studies on MB adsorption onto activated carbons report equilibrium within a few hours; however, two-stage kinetic profiles have been observed in highly porous or heterogeneous adsorbents. In such systems, the kinetic behavior has been associated with a micro/mesoporous structure and surface heterogeneity providing binding sites of different energies [21,53]. In the present case, the slower second stage likely reflects the progressive penetration of MB molecules into micropores and interaction with higher-energy sites. Similar biphasic uptake, characterized by rapid external diffusion followed by slower intraparticle penetration, has been reported for micro/mesoporous carbonaceous adsorbents [5], for diffusion models describing a transition from film diffusion control to intraparticle diffusion as adsorbates move deeper into the pore network [45]. Studies on modified biochars and hybrid or polymer–carbon adsorbents also describe analogous shifts between film-diffusion and intraparticle-diffusion regimes, indicating that pore-structure heterogeneity and the distribution of adsorption energies can give rise to a slow terminal kinetic region [54,55]. Taken together, these observations are consistent with a sequential occupation of external, mesoporous and finally microporous domains in M300.

Therefore, while 36 h is substantially longer than typically reported, adopting this extended contact ensured that adsorption capacities were not underestimated and that isotherm modeling was conducted under genuine equilibrium conditions [43].

Applying the data obtained from the adsorption kinetics experiments to the established kinetic models yielded the parameters shown in Table 4. In the case of M300, biphasic adsorption phases were observed: a first phase up to 6 hours of equilibrium time, and a second extending to 36 hours.

Both biochars, P260 and M300, showed the best fit with the pseudo-second order kinetic model, where the adsorption rate has a quadratic relationship with the variation in total and partial adsorption capacity at a given time t [45]. The best fit of this model for MB adsorption onto biochar was viewed in other articles [5,21,56]. M300 also showed the highest correlation with the pseudo-second-order model; however, the correlation was stronger when the data were split into two time ranges (before and after 6 hours) than when modeled together. Both the pseudo-first-order and Elovich models also showed good fits for the M300 data, with R^2 values exceeding 0.90 for all data sets and above 0.95 for the adsorption data after 6 hours.

Table 4. Kinetic parameters of Pseudo-first and second order, Intraparticle diffusion and Elovich models.

	Pseudo-first order			Pseudo-second order			Intraparticle diffusion		Elovich		
	R^2	Qe	K_1	R^2	Qe	K_2	R^2	K_i	R^2	α	β
P260 24h	0,482	1,60	-0,8733	**0,992**	**8,285**	**0,0673**	0,624	0,0017	0,855	1,19	1,43
M300 36h	0,974	19,10	0,0013	**0,987**	**32,982**	**0,0096**	0,819	0,0072	0,942	2,51	0,21
M300 (0-6h)	0,738	18,88	0,0011	**0,997**	**18,450**	**0,0891**	0,507	0,0336	0,908	2,17	0,37
M300 (6-36h)	0,956	18,92	0,0013	**0,996**	**35,881**	**0,0053**	0,839	0,0050	0,953	2,87	0,15

To further elucidate this behavior, the kinetic data were segmented into two intervals: 0–6 h and 6–36 h. In both stages, the pseudo-second-order model provided the best fit, with R^2 values of 0.997 and 0.996, respectively. While the good agreement between experimental and calculated q_e values supports the suitability of this model, which by itself does not prove chemisorption, it suggests that the adsorption rate is strongly dependent on the availability of active sites, a feature that is often, but not exclusively, associated with stronger interactions such as surface complexation, π–π interactions, or electrostatic attraction [5,6].

The Weber–Morris intraparticle diffusion model provided additional insight. The plots exhibited two distinct linear regions with non-zero intercepts, indicating that intraparticle diffusion played a significant role but was not the sole rate-limiting step. The initial steeper region (0–6 h) corresponds to external film diffusion and rapid surface uptake, whereas the second, gentler slope (6–36 h) reflects a slower intraparticle diffusion regime associated with the penetration of MB molecules into micro- and mesopores [57,58]. The non-zero intercepts confirm that boundary-layer resistance remained relevant throughout the process. Such multilinearity in Weber–Morris plots is commonly interpreted as evidence for a multi-step mechanism involving both film and pore diffusion [59].

Although the intraparticle diffusion plots (Weber–Morris) did not show perfect correlation (R^2 = 0.507–0.839), the multilinearity and non-zero intercepts indicate that intraparticle diffusion contributed to the adsorption process but was not the sole rate-controlling mechanism [57-59]. This is consistent with the biphasic uptake observed and with the pseudo-second order fittings, which point to a surface-controlled process complemented by diffusion limitations [58]. Taken together, these results indicate that the extended equilibration time of M300 arises from the sequential operation of different mass transfer regimes [53]. The fast initial stage rapidly saturates accessible external and mesoporous sites, while the slow stage involves diffusion into smaller pores and interaction with higher-energy or less accessible sites, prolonging the approach to equilibrium. Although less frequently reported for MB adsorption, the biphasic behavior has been described in porous and heterogeneous adsorbents, particularly when micropores or narrow channels dominate the textural structure [5,21]. By adopting 36 h as the equilibrium contact time, it was ensured that adsorption capacities were not underestimated and that isotherm modeling reflected final equilibrium conditions.

3.5. Adsorption of MB in Mixtures of P260 and M300

3.5.1. Multivariate Analysis at Shorter Equilibrium Time

The three-dimensional response surface plots and contour plots obtained from the multivariate analysis experiments are shown in Figure 7. The correlation coefficients (R^2) were 0.9127 for Qe and 0.9035 for Qe – Qt, indicating that the model created from the multivariate analysis has a satisfactory correlation above 90% with the experimental data.

Both the Qe and Qe – Qt graphs exhibit the same trends, showing a parabolic shape along the %M300 axis. There is an increase in Qe and Qe – Qt as the proportion of modified biochar in the adsorbent increases, reaching a maximum point after which the values begin to decline. Along the equilibrium time axis, there is a consistent increase in Qe and Qe – Qt with longer contact time between MB and the adsorbent.

In the contour plots of Qe – Qt (Figure 7d), some regions showed values lower than the theoretical value based solely on P260, indicating that at low percentages of M300 and shorter equilibrium times, the addition of the modified biochar has an antagonistic effect on adsorption capacity. However, due to the significantly higher adsorption capacity of M300 compared to P260, Qe – Qt increases with the amount of modified biochar incorporated into the adsorbent, and its addition begins to have a positive effect on adsorption performance. The conditions under which the addition of M300 exerts a positive effect are highlighted in orange and red on the contour plot, with M300 ranging from 10% to 35% across most of the equilibrium time range studied.

The table of regression coefficients, Student's t values, and p-values is shown in Table 5. The Student's t-test and p-value are used to identify which factors are most significant in a model. The Student’s t statistic quantifies the relative importance of each factor, where higher absolute t values indicate greater significance. When the calculated t values exceed the critical table value, the factor is considered statistically significant. Similarly, the p-value provides a comparative measure, where lower p-values reflect stronger statistical significance [46]. In this model, a 95% confidence level was adopted, using the critical t value corresponding to a 5% significance level and a maximum acceptable p-value of 0.05, where factors with t values greater than the critical threshold and p values lower than 0.05 were deemed significant [43,46]. In both cases (Qe and Qe − Qt), the percentage of M300 was more significant than equilibrium time. The %M300 factor showed both linear and quadratic significance in both response variables, while time was only marginally significant in the linear term for Qe—with t slightly above the critical value and p-value just below 0.05—and was not significant for Qe − Qt. This aligns with the response surface analysis, where greater variation was observed along the %M300 axis, while changes along the time axis were smaller. The interaction term (time × %M300) and the lack-of-fit parameter were not significant for either Qe or Qe − Qt, suggesting no interaction effect between the factors and confirming that the model provides a good fit to the observed data.

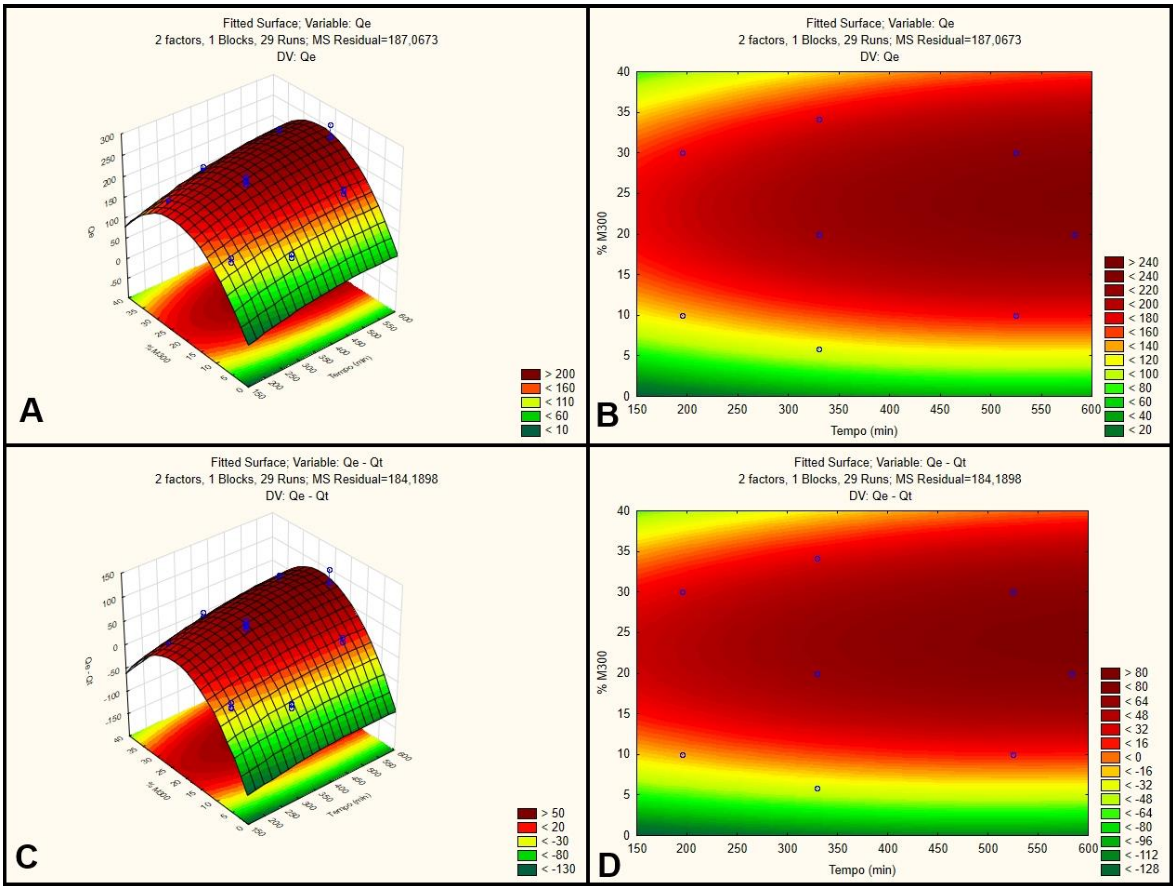

Figure 7. Fitted response surfaces of (a) Qe and (c) Qe – Qt and contour plots of (b) Qe and (d) Qe – Qt.

Table 5. Regression coefficients, formula and statistical parameters of the experimental design.

	Qe					Qe - Qt				
Factor	Regr.	Error	t calc.	t tab.	p-values	Regr.	Error	t calc.	t tab.	p-values
Inters.	-39,4616	32,5450	-1,21	2,08	0,239	**-165,158**	**32,5450**	**-5,07**	**2,08**	**0,000**
Time (L)	**0,3135**	**0,1480**	**2,12**	**2,08**	**0,046**	0,2104	0,1481	1,42	2,08	0,170
Time (Q)	-0,0003	0,0002	-1,65	2,08	0,113	-0,0002	0,0002	-1,18	2,08	0,253
%M300 (L)	**15,0792**	**1,6757**	**9,00**	**2,08**	**0,000**	**14,9841**	**1,6757**	**8,94**	**2,08**	**0,000**
%M300 (Q)	**-0,3369**	**0,0348**	**-9,67**	**2,08**	**0,000**	**-0,3347**	**0,0348**	**-9,61**	**2,08**	**0,000**
Time x %M300	0,0023	0,0025	0,89	2,08	0,384	0,0023	0,0025	0,89	2,08	0,382
Equation	$Y = 0{,}3135\,X_1 + 15{,}0792\,X_2 - 0{,}3369\,X_2^2$					$Y = -165{,}1587 + 14{,}9841\,X_2 - 0{,}3347\,X_2^2$				

The desirability functions for the responses Qe and Qe – Qt are shown in Figure 8. It was observed that the optimal point occurs at 27.07% of M300 in the adsorbent and a contact time of 583 minutes. Under these conditions, the adsorption capacity (Qe) is 238.71 mg g^{-1}, and the difference between theoretical and experimental adsorption capacities (Qe – Qt) is 81.425 mg g^{-1}.

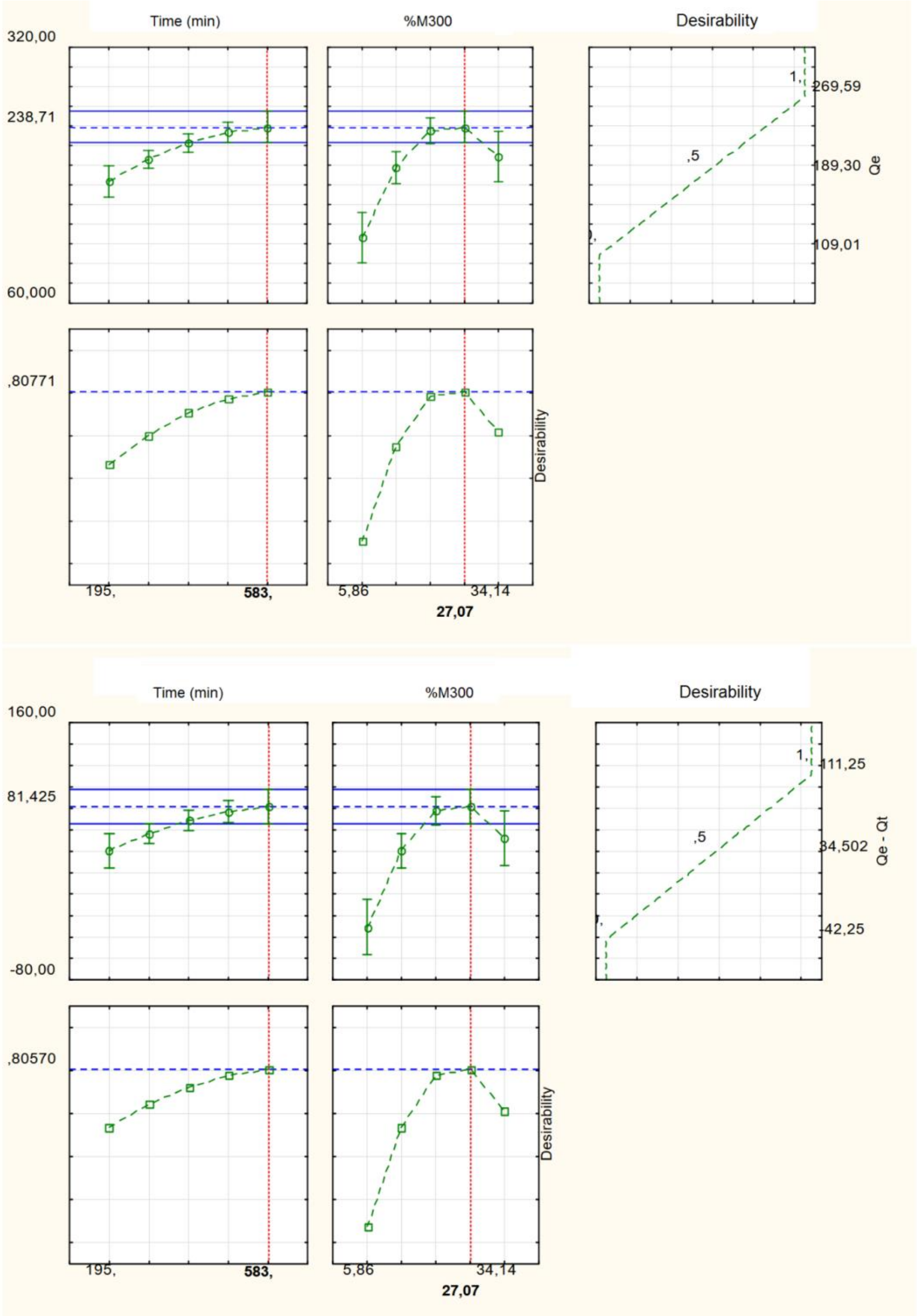

Figure 8. Predicted values and optimal parameters from the multivariate analysis for Qe and Qe-Qt.

However, it is important to highlight that the optimal time corresponded to the upper boundary of the experimental range. This limitation suggests that the equilibrium had not been fully achieved, particularly for M300, as indicated by its biphasic adsorption kinetics. Similar findings have been reported where intraparticle diffusion processes extend equilibration beyond the time windows initially considered in optimization studies [5,43]. Consequently, although the desirability function provided an operational optimum, further experiments extending the contact time are recommended to validate the true optimal point and confirm maximum system performance [53,54].

Despite this, it was possible to establish a reliable optimal value for the proportion of modified biochar, supporting the recommendation of using mixtures with around 27% M300 as a strategy to balance high adsorption efficiency and minimize potential impacts associated with chemical activation.

3.5.2. Multivariate Analysis at Longer Equilibrium Time

The response surface and contour plots from the multivariate analysis performed at longer equilibrium times are shown in Figure 9a and 9b, respectively. The model presented a coefficient of determination (R^2) of 0.9223, indicating a satisfactory correlation above 90% with the observed data.

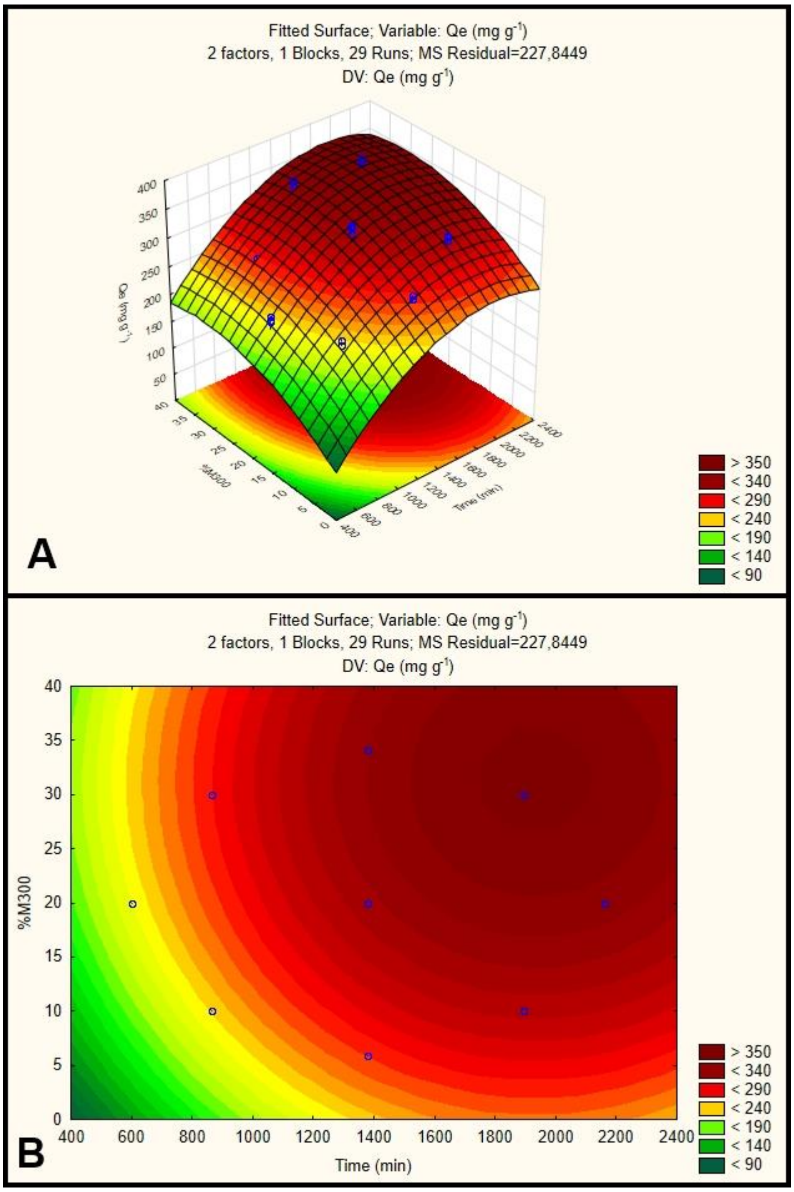

Figure 9. (a) Fitted surface of response of Qe and (b) and contour plots of Qe.

The response surface for adsorption capacity (Qe) shows a negative-definite matrix with downward convexity, meaning there is a stationary maximum point, which corresponds to the maximum experimental adsorption capacity. The model achieved optimization, as it was able to determine the point of maximum adsorption within the evaluated ranges of equilibrium time and percentage of modified biochar (M300) in the adsorbent mixture. In this analysis, a greater influence of equilibrium time on adsorption capacity was observed compared to the previous multivariate analysis with shorter contact times (up to 10 hours). The increase in Qe with increasing contact time is much more pronounced in this case. The region of highest adsorption capacity in the contour plot is located between 1800 and 2000 minutes, with M300 proportions between 27% and 35%.

The regression coefficients, Student's t-values, and p-values are presented in Table 6. As in the previous multivariate analysis, a confidence level of 95% was adopted, where the critical t-values represent the 5% significance threshold, and the maximum accepted p-value was 0.05 [46]. Both the equilibrium time and the percentage of M300 were significant factors in the model, in both their linear and quadratic forms, with t-values greater than the critical value and p-values lower than 0.05. The interaction term (Time × %M300) and the lack-of-fit parameter were not significant, indicating that the two variables do not exhibit interdependence in their effects on adsorption capacity and that the model fits the observed data well.

Table 6. Regression coefficients, formula and statistical parameters of the experimental design.

Factor	Regression	Error	t calc.	t tab.	p-values
Intersection	-13,1432	40,46564	-0,32	2,08	0,748268
Time (L)	**0,2799**	**0,04209**	**6,65**	**2,08**	**0,000001**
Time (Q)	**-0,0001**	**0,00001**	**-5,25**	**2,08**	**0,000025**
%M300 (L)	**6,6887**	**2,07271**	**3,23**	**2,08**	**0,003730**
%M300 (Q)	**-0,1072**	**0,04272**	**-2,51**	**2,08**	**0,019618**
Time x %M300	0,0000	0,00084	0,02	2,08	0,982073
Equation	$Y = 0{,}2799\ X_1 - 0{,}0001\ X_1^2 + 6{,}6887\ X_2 - 0{,}1072\ X_2^2$				

The desirability functions for Qe are shown in Figure 10. The plots reveal that higher equilibrium times (between 1770 and 2160 minutes) and M300 proportions (between 27.07% and 34.14%) correspond to the regions with the highest adsorption capacities. The optimal values for M300 content and equilibrium time were 34.14% and 1770 minutes, respectively. However, the variation in adsorption capacity within the ranges of 1770–2160 minutes and 27.07%–34.14% is small and falls within the standard deviation of both points.

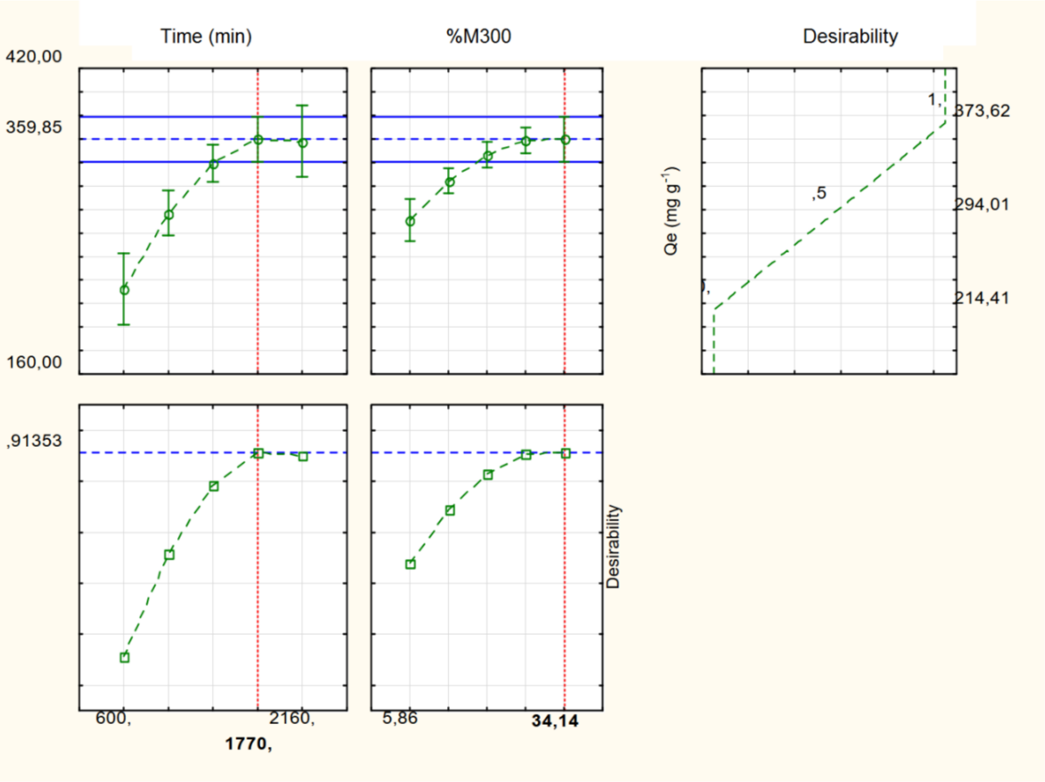

Figure 10. Profiles of the predicted values and optimal parameters from the multivariate analysis.

From a process-design standpoint, the optimization results presented in Figure 10 are particularly relevant. They show that mixtures containing around 30% of M300 and the remaining fraction of P260 can reach equilibrium adsorption capacities above 350 mg g^{-1} within the studied time window of 36 hours. In practice, this means that high dye-removal efficiencies can be achieved without relying exclusively on fully activated biochar, which reduces the amount of chemically modified material that must be produced and handled.

These results therefore provide a basis for selecting mixture compositions that balance adsorption capacity and the proportion of activated biochar in potential treatment systems with low cost and more environmentally friendly. The use of Pinus elliottii strobili, a forestry residue that is often discarded without a defined end use, provides an abundant and low-cost precursor, while activation at relatively low temperatures (260–300 °C) is expected to reduce energy demand compared with conventional high-temperature pyrolysis. In addition, the optimization results indicate that mixtures containing only about 30% of fully activated M300 can achieve equilibrium capacities above 350 mg g^{-1}, which implies lower phosphoric-acid consumption and a smaller amount of chemically modified material to be produced and managed. This performance–cost–environment trade-off is a key aspect to be considered when moving from laboratory-scale tests to real treatment systems.

However, some relevant limitations of this study must also be acknowledged. All adsorption experiments were carried out in synthetic, single-solute methylene blue solutions under controlled pH and temperature, in batch mode and with relatively long contact times, especially for M300. No BET surface area or pore-size distribution measurements were obtained in this study, and the effect of pH on the performance of the mixtures was not systematically evaluated. Regeneration and multi-cycle reuse of the adsorbents, as well as possible leaching of phosphorus and other inorganic elements, were also not addressed. Future work should therefore investigate the behavior of these materials in continuous-flow systems and real wastewaters, including competitive adsorption, regeneration and stability over repeated cycles, leaching tests and supporting life cycle and techno-economic analyses to better define their feasibility for large-scale implementation.

4. Conclusion

This study demonstrated that phosphoric acid activation of Pinus elliottii strobili biochar markedly enhances its performance as an adsorbent for cationic contaminants. The Langmuir maximum adsorption capacity (Qmax) increased from 274.68 mg g^{-1} for the unmodified low-temperature biochar (P260) to 508.02 mg g^{-1} for the activated M260 and 685.72 mg g^{-1} for the biochar activated at 300 °C (M300), whereas anthracite coal (C_{ant}) reached only 86.18 mg g^{-1}. FTIR, SEM, and pHPZC analyses revealed structural and surface features favorable to dye uptake, and kinetic results confirmed that both P260 and M300 follow a pseudo-second-order model, with P260 reaching equilibrium within 360–540 min and M300 exhibiting a biphasic uptake pattern consistent with sequential film and intraparticle diffusion. Mixture-design experiments further demonstrated that blends containing approximately 27–34% M300 achieved equilibrium capacities close to 360 mg g^{-1} at contact times of 1770 min, confirming the potential of mixed systems to combine high performance with reduced use of activated material.

Altogether, these results highlight the potential of *P. elliottii* strobili, a widely available forestry residue, as a low-cost precursor for low-temperature, phosphoric acid–activated biochars suitable for water treatment applications, based on simple and scalable processing steps. Nevertheless, this work is subkect by relevant constraints: all experiments were conducted in batch reactors with synthetic, single-solute methylene blue solutions and relatively long contact times; no BET surface area or pore size distribution measurements were obtained; and the influence of pH on the performance of the mixtures was not systematically evaluated. Regeneration, multi-cycle reuse and possible leaching of phosphorus and other inorganic elements were also not addressed. Future research should therefore assess these biochars in continuous-flow systems and real effluents containing multiple contaminants, combined with regeneration, stability and leaching studies, as well as complementary textural and surface characterizations, to better define their environmental safety and feasibility for large-scale wastewater treatment.

Author Contributions: Conceptualization, C.A.R., M.A.S. and I.A.P.F.; methodology, M.A.S.; formal analysis, C.A.R., M.A.S. and I.A.P.F.; resources, C.A.R.; writing—original draft preparation, M.A.S. and C.A.R.; writing—review and editing, C.A.R., M.A.S. and I.A.P.F.; supervision, C.A.R; project administration and funding acquisition, C.A.R.

Data availability statement: Data are available from the corresponding author upon request.

Conflict of Interest: The authors declare no conflict of interest.

Acknowledgments: The authors would like to express their sincere gratitude to the Thermal Analysis Laboratory at UNESP–Araraquara for the support and access to its facilities. We also thank all individuals and institutions who contributed directly or indirectly to the development of this research.

References

[1] Wang, X., Guo, Z., Hu, Z., & Zhang, J. (2020). Recent advances in biochar application for water and wastewater treatment: A review. *PeerJ*, *8*, e9164. https://doi.org/10.7717/peerj.9164

[2] Tundisi, J. G. (2008). Recursos hídricos no futuro: problemas e soluções. *Estud. Avançados*, *22*(63), 7–16. https://doi.org/10.1590/S0103-40142008000200002

[3] Baird, C. (2002). *Química ambiental* (2nd ed.). Bookman.

[4] Crini, G. (2006). Non-conventional low-cost adsorbents for dye removal: A review. *Bioresour. Technol.*, *97*(9), 1061–1085. https://doi.org/10.1016/j.biortech.2005.05.001

[5] Wei, F., Chen, R., Hu, X., Lei, B., Liu, T., Hao, M., Chen, Y., Ding, Y., & Luo, X. (2023). Revealing the combined effect of active sites and intra-particle diffusion on adsorption mechanism of methylene blue on activated red-pulp pomelo peel biochar. *Materials*, *16*(9), 3546. https://doi.org/10.3390/ma16093546

[6] Ceroni, L., Benazzato, S., Pressi, S., Calvillo, L., Marotta, E., & Menna, E. (2024). Enhanced adsorption of methylene blue dye on functionalized multi-walled carbon nanotubes. *Nanomaterials*, *14*(6), 522. https://doi.org/10.3390/nano14060522

[7] Sultana, M., Rownok, M. H., Sabrin, M., Rahaman, M. H., & Nur Alam, S. P. (2022). A review on experimental chemically modified activated carbon to enhance dye and heavy metals adsorption. *Cleaner Eng. Technol.*, *6*, 100382. https://doi.org/10.1016/j.clet.2021.100382

[8] Ahmed, A., Bashir, A., Shah, S. A. A., & Zhang, Z. (2024). Impact of coal energy development on the surrounding water bodies. *Sci. Total Environ.*, *916*, 170263. https://doi.org/10.1016/j.scitotenv.2024.170263

[9] Koppe, J. C., & Costa, J. F. C. L. (2008). A lavra de carvão e o meio ambiente em Santa Catarina. In M. A. S. da Luz (Ed.), *Carvão Brasileiro: tecnologia e meio ambiente* (1st ed.).

[10] Campos, M. L., Almeida, J. A., Silveira, C. B., Gatiboni, L. C., Albuquerque, J. A., Mafra, A. L., et al. (2010). Impactos no solo provocados pela mineração e depósito de rejeitos de carvão mineral. *Rev. Ciênc. Agron. Vet.*, *9*(2), 198–205.

[11] Kumar, A., Yadav, P., Kumar, A., & Krishnan, V. (2022). Coal fly ash: An emerging material for water remediation. *J. Sustain. Min.*, *21*(1), 57–70. https://doi.org/10.1007/s40789-022-00512-1

[12] Chen, H., Li, W., Wang, J. J., Xu, H. J., Liu, Y. L., Zhang, Z., et al. (2019). Adsorption of cadmium and lead ions by phosphoric-acid-modified biochar generated from chicken feather. *Bioresour. Technol.*, *292*, 121948. https://doi.org/10.1016/j.biortech.2019.121948

[13] Jung, C., Boateng, L. K., Flora, J. R. V., Oh, J., Braswell, M. C., Son, A., et al. (2015). Competitive adsorption of selected non-steroidal anti-inflammatory drugs on activated biochars. *Chem. Eng. J.*, *264*, 1–9. https://doi.org/10.1016/j.cej.2014.11.076

[14] Moreira, M. T., Noya, I., & Feijóo, G. (2017). The prospective use of biochar as adsorption matrix – A review from a lifecycle perspective. *Bioresour. Technol.*, *246*, 135–141. https://doi.org/10.1016/j.biortech.2017.08.041

[15] Wang, Y., Chen, L., Zhu, Y., Fang, W., Tan, Y., He, Z., & Liao, H. (2024). Research status, trends, and mechanisms of biochar adsorption for wastewater treatment: A scientometric review. *Environ. Sci. Eur.*, *36*, 25. https://doi.org/10.1186/s12302-024-00859-z

[16] Zhou, Y., Wu, C., Xu, Z., & Zhao, Y. (2024). Innovations and challenges in adsorption-based wastewater treatment. *Heliyon*, *10*(5), e28014. https://doi.org/10.1016/j.heliyon.2024.e28014

[17] Maneechakr, P., & Karnjanakom, S. (2024). Adsorptive removal of methylene blue by bio-based adsorbents: Mechanisms, performance and challenges. *Physicochem. Probl. Miner. Process.*, *60*, 176509. https://doi.org/10.37190/ppmp/176509

[18] He, R., Hui, K., Zhang, X., & Yao, H. (2024). Insight into the role of the pore structure and surface functional groups in biochar on the adsorption of sulfamethoxazole from synthetic urine. *Appl. Sci.*, *14*(5), 1715. https://doi.org/10.3390/app14051715

[19] Calazans, T. R. N. M., de Freitas, A. M., de Souza, M. A. A., da Silva, L. A., da Silva, L. F., dos Santos, J. R., da Rocha, A. C. V., de Souza, A. G., da Silva, D. L., & de Oliveira, M. C. M. (2024). Methylene blue removal using a nanomagnetic support: A response surface approach. *Nanoscale Adv.*, *6*, 3887–3894. https://doi.org/10.1039/D4NA00318G

[20] Santoso, E., Ediati, R., Kusumawati, Y., Bahruji, H., Sulistiono, D. O., & Prasetyoko, D. (2020). Review on recent advances of carbon-based adsorbent for methylene blue removal from wastewater. *Mater. Today Chem.*, *16*, 100233. https://doi.org/10.1016/j.mtchem.2019.100233

[21] Zaidi, A. G., Azemi, M. T. H. R., Yaacob, M. H., Uyup, N. H., Ang, L. S., & Akbar, N. A. (2022). Adsorption of methylene blue from aqueous solutions by activated carbon prepared from banana trunk using zinc chloride activation. *Malays. J. Anal. Sci.*, *26*(2), 384–398. https://mjas.analis.com.my/mjas/v26_n2/pdf/Zaidi_26_2_17.pdf

[22] Cwalinski, J., Wróblewska, M., Wróbel, T. M., Latacz, G., Handzlik, J., Filipek, B., Król, M., Gawlik, K., Wojnar, W., & Strzelczyk, A. (2020). Methylene blue—Current knowledge, fluorescent properties, and its future use. *Diagnostics*, *10*(7), 583. https://doi.org/10.3390/diagnostics10070583

[23] Bhomick, P. C., Supong, A., Baruah, M., Pongener, C., & Sinha, D. (2018). Pine cone biomass as an efficient precursor for the synthesis of activated biocarbon for adsorption of anionic dye: Isotherm, kinetic, thermodynamic and regeneration studies. *Sustain. Chem. Pharm.*, *10*, 41–49. https://doi.org/10.1016/j.scp.2018.09.001

[24] Dawood, S., Sen, T. S., & Phan, C. (2017). Synthesis and characterization of slow-pyrolysis pine-cone biochar in the removal of pollutants: Kinetic, equilibrium, mechanism and thermodynamic study. *Bioresour. Technol.*, *246*, 76–81. https://doi.org/10.1016/j.biortech.2017.07.019

[25] Mahmoodi, N. M., Hayati, B., Arami, M., & Lan, C. (2011). Adsorption of textile dyes on pine cone from coloured wastewater: Kinetic, equilibrium and thermodynamic studies. *Desalination*, *268*(1–3), 117–125. https://doi.org/10.1016/j.desal.2010.10.007

[26] Di Domenico, A., Tamagnini, T., Paolucci, C., et al. (2024). New frontiers for raw wooden residues: Biochar production as a resource for environmental challenges. *J. Carbon Res.*, *10*(2), 54. https://doi.org/10.3390/c10020054

[27] Sizmur, T., Fresno, T., Gökçen, A., Frost, H., & Jiménez, E. M. (2017). Biochar modification to enhance sorption of inorganics from water. *Bioresour. Technol.*, *246*, 34–47. https://doi.org/10.1016/j.biortech.2017.07.082

[28] Gokce, Y., Savas, Y., Emine, Y., Banford, A., & Aktas, Z. (2021). Adsorption behaviour of high-performance activated carbon from demineralised low-rank coal (Rawdon). *J. Environ. Chem. Eng.*, *9*(2), 104819. https://doi.org/10.1016/j.jece.2020.104819

[29] Yangmur, E., Ozmak, M., & Aktas, Z. (2008). A novel method for production of activated carbon from waste tea using microwave activation. *Fuel*, *87*(15–16), 3278–3285. https://doi.org/10.1016/j.fuel.2008.05.005

[30] Pongkua, W., Dolphern, R., & Thiravetyan, P. (2020). Bioremediation of gaseous methyl tert-butyl ether using sulfuric-acid-modified bagasse activated carbon–bone biochar beads. *Chemosphere*, *239*, 124724. https://doi.org/10.1016/j.chemosphere.2019.124724

[31] Wang, T., Wu, J., Zhang, Y., Liu, J., Sui, Z., Zhang, H., et al. (2018). Increasing chlorine active sites in micropores of biochar for improved mercury adsorption. *Fuel*, *229*, 60–67. https://doi.org/10.1016/j.fuel.2018.05.028

[32] Tan, X. F., Liu, Y. G., Gu, Y. L., Xu, Y., Zeng, G. M., Hu, X. J., et al. (2016). Biochar-based nanocomposites for the decontamination of wastewater: A review. *Bioresour. Technol.*, *212*, 318–333. https://doi.org/10.1016/j.biortech.2016.04.093

[33] Reddy, K. S. K., Al Shoaibi, A., & Srinivasakannan, C. (2012). A comparison of microstructure and adsorption characteristics of activated carbons from date-palm pits. *New Carbon Mater.*, *27*(5), 344–351. https://doi.org/10.1016/S1872-5805(12)60020-1

[34] Girgis, B. S., & El-Hendawy, A. A. (2002). Porosity development in activated carbons obtained from date pits under chemical activation with phosphoric acid. *Microporous Mesoporous Mater.*, *52*(2), 105–117. https://doi.org/10.1016/S1387-1811(01)00481-4

[35] El-Gamal, E., Khedr, M., & Rashad, M. (2023). Corncob biochar activation by phosphoric acid and hydrogen peroxide for enhancing ammonium adsorption. *Int. J. Adv. Sci. Res. Innov.*, *6*(2), 27–44. https://doi.org/10.21608/ijasri.2023.236421.1007

[36] Danish, M., & Ahmad, T. (2018). A review on utilization of wood biomass as a sustainable precursor for activated carbon production and application. *Renew. Sustain. Energy Rev.*, *82*, 3003–3039. https://doi.org/10.1016/j.rser.2017.10.004

[37] Neme, I., Gonfa, G., Masi, C., et al. (2023). Activated carbon from biomass precursors using phosphoric acid: A review. *Membranes*, *13*(4), 365. https://doi.org/10.3390/membranes13040365

[38] Han, Y., Yin, Y. M., Zhang, H., Sun, S. J., Huang, Z. Z., Deng, Y. S., & Bao, L. (2024). Adsorption effect of phosphate-modified grape-branch biochar on Cd^{2+}. *J. Geosci. Environ. Prot.*, *12*, 59–77. https://doi.org/10.4236/gep.2024.124005

[39] Qiu, C., Wang, C., Liu, Q., Gao, M., & Song, Z. (2023). Effective removal of Cd from aqueous solutions using P-loaded Ca–Mn-impregnated biochar. *Molecules*, *28*(22), 7553. https://doi.org/10.3390/molecules28227553

[40] Ge, Q., Tian, Q., Wang, S., Zhang, J., & Hou, R. (2022). Highly efficient removal of lead/cadmium by H_3PO_4-modified hydrochar prepared from banana peels. *Langmuir*, *38*(12), 3907–3915. https://doi.org/10.1021/acs.langmuir.2c02693

[41] Pantano, G., Grosseli, G. M., Mozeto, A. A., & Fadini, P. S. (2016). Sustentabilidade no uso do fósforo: Uma questão de segurança hídrica e alimentar. *Quím. Nova*, *39*(6), 732–740. https://doi.org/10.5935/0100-4042.20160086

[42] Itodo, A. U., Itodo, H. U., & Gafar, M. K. (2010). Estimation of specific surface area using Langmuir isotherm method. *J. Appl. Sci. Environ. Manage.*, *14*(4), 141–145. https://doi.org/10.4314/jasem.v14i4.63287

[43] Al-Ghouti, M. A., & Da'ana, D. A. (2020). Guidelines for the use and interpretation of adsorption isotherm models: A review. *J. Hazard. Mater.*, *393*, 122383. https://doi.org/10.1016/j.jhazmat.2020.122383

[44] Oscik, J. (1982). *Adsorption*. Ellis Horwood.

[45] Russo, V., Tesser, R., Trifuoggi, M., Giugni, M., & Di Serio, M. (2015). A dynamic intraparticle model for fluid–solid adsorption kinetics. *Comput. Chem. Eng.*, *74*, 66–74. https://doi.org/10.1016/j.compchemeng.2015.01.001

[46] Zolgharnein, J., Shahmoradi, A., & Ghasemi, J. (2013). Comparative study of Box–Behnken, central composite, and Doehlert matrix for optimization of Pb(II) adsorption onto Robinia leaves. *J. Chemom.*, *27*(1–2), 12–20. https://doi.org/10.1002/cem.2487

[47] Fan, M., Dai, D., & Huang, B. (2012). Fourier transform infrared spectroscopy for natural fibres. In S. M. Salih (Ed.), *Fourier transform – Materials analysis*. IntechOpen.

[48] Herrera, R., Erdocia, X., Llano-Ponte, R., & Labidi, J. (2014). Characterization of hydrothermally treated wood in relation to changes on its chemical composition and physical properties. *J. Anal. Appl. Pyrolysis*, *107*, 256–266. https://doi.org/10.1016/j.jaap.2014.03.010

[49] Kauffman, K. L., Culp, J. T., Goodman, A., & Matranga, C. (2011). FT-IR study of CO_2 adsorption in a dynamic copper(II) benzoate-pyrazine host. *J. Phys. Chem. C*, *115*(5), 1857–1866. https://doi.org/10.1021/jp102273w

[50] Chu, G., Zhao, J., Huang, Y., Zhou, D. D., Liu, Y., Wu, M., et al. (2018). Phosphoric acid pretreatment enhances the specific surface areas of biochars by generation of micropores. *Environ. Pollut.*, *240*, 1–9. https://doi.org/10.1016/j.envpol.2018.04.003

[51] Peng, H. B., Gao, P., Chu, G., Pan, B., Peng, J. H., & Xing, B. S. (2017). Enhanced adsorption of Cu(II) and Cd(II) by phosphoric-acid-modified biochars. *Environ. Pollut.*, *229*, 846–853. https://doi.org/10.1016/j.envpol.2017.07.004

[52] Zhang, H., Liu, X., Wang, Y., Cao, Q., & Liu, L. (2020). Enhanced adsorption of malachite green from aqueous solution by rice straw-derived biochar activated by phosphoric acid. *Ecotoxicol. Environ. Saf.*, *200*, 110025. https://doi.org/10.1016/j.ecoenv.2020.110025

[53] Liu, H., Zhu, J., Li, Q., Li, L., Huang, Y., Wang, Y., Fan, G., & Zhang, L. (2023). Adsorption performance of methylene blue by KOH/$FeCl_3$ modified biochar/alginate composite beads derived from agricultural waste. *Molecules*, *28*(6), 2507. https://doi.org/10.3390/molecules28062507

[54] Moradeeya, P. G., Kumar, M. A., Sharma, A., & Basha, S. (2025). Sequential sorption-photocatalytic method using polypyrrole@TiO_2 nanocomposites for the removal of agrochemicals. *Indian J. Chem. Technol.*, *32*(3), 395–406. https://doi.org/10.56042/ijct.v32i3.8911

[55] Nama, M., Satasiya, G., Sahoo, T. P., Moradeeya, P. G., Sadukha, S., Singhal, K., Saravaia, H. T., Dineshkumar, R., & Kumar, M. A. (2024). Thermo-chemical behaviour of Dunaliella salina biomass and valorising their biochar for naphthalene removal from aqueous rural environment. *Chemosphere*, *353*, 141639. https://doi.org/10.1016/j.chemosphere.2024.141639

[56] Charmas, B., Wawrzaszek, B., & Jedynak, K. (2023). Biochars from wood biomass as effective methylene blue adsorbents. *Physicochem. Probl. Miner. Process.*, *59*(4), 176509. https://doi.org/10.37190/ppmp/176509

[57] Gonçalves dos Santos, M., Paquini, L. D., Quintela, P. H. L., Profeti, L. P. R., & Guimarães, D. (2025). Insights into kinetics and thermodynamics for adsorption methylene blue using ecofriendly zeolites materials. *ACS Omega*, *10*(20), 20326–20340. https://doi.org/10.1021/acsomega.4c11718

[58] López-Luna, J., Ramírez-Montes, L. E., Martinez-Vargas, S., Martínez, A. I., Mijangos-Ricardez, O. F., González-Chávez, M. del C. A., Carrillo-González, R., Solís-Domínguez, F. A., Cuevas-Díaz, M. del C., & Vázquez-Hipólito, V. (2019). Linear and nonlinear kinetic and isotherm adsorption models for arsenic removal by manganese ferrite nanoparticles. *SN Appl. Sci.*, *1*, 950. https://doi.org/10.1007/s42452-019-0977-3

[59] Bogyor, A., Csavdari, A. A., Lovász, T., & Bitay, E. (2025). A comparative kinetic and thermodynamic adsorption study of methylene blue and its analogue dye on filter paper. *Int. J. Mol. Sci.*, *26*(2), 516. https://doi.org/10.3390/ijms26020516